# Test of the Multi-Anode PMT Hamamatsu H8500 for the CLAS12 RICH

June 22, 2013

# Contents


**1 Photon detectors for the RICH** **3**

**2 Single photon response** **3**

**3 Cross talk** **6**

**4 Gain analysis** **7**

**5 Dark current analysis** **9**

# 1 Photon detectors for the RICH

There are several requirements limiting the choice of photon detector. For instance, the photon detector must provide a spatial resolution of less than 1 cm. Due to the imaging aspect of the RICH and since multiple photon detectors will be tiled into large arrays, it is crucial that the photon detector provides an active area with minimal deadspace. The photon detector must also efficiently detect single photon level signals and, due to the aerogel radiator material, should be sensitive in visible light wavelengths.

MultiAnode PhotoMultiplier Tubes (MAPMTs) exist as promising candidates for the CLAS12 RICH and the currently selected photon detector is the flat-panel Hamamatsu H8500 MAPMT, which offers an adequate compromise between detector performance and cost. The H8500 MAPMT comprises an $8 \times 8$ array of pixels, each with dimensions $5.8 \times 5.8$ mm$^2$, into an active area of $49.0 \times 49.0$ mm$^2$. Furthermore, the device has a very high packing fraction of 89%.

These MAPMTs are not advertised as the optimal choice for single photon detection, while other tubes, specifically designed this regime (as for example the R8900 or the new R11625), are much more expensive in terms of cost per unit area. For this reason, detailed studies to characterize the response of the H8500 have been performed.

The H8500 are produced in two versions, the H8500C with normal glass entrance window and the H8500C-03 with UV-enhanced glass window. The quantum efficiency of these two tubes are shown in Fig. 1. It is maximal in the blue light region, thus matching the emission spectrum of Cherenkov light in the aerogel.

# 2 Single photon response

The response of 28 H8500 phototubes (14 of each of the two version) to a low intensity photon beam was done by using a laser emitting blue light, remotely controlled to scan the MAPMT surface, and standard VME electronics for the readout. The set-up was installed inside a *black box* to isolate the MAPMT from any background light (see [1] for further details).

The intensity of the laser was reduced at a few photons per pulse by adjusting the tune of the laser and by using neutral density filters. With the two motors, the laser was moved across the MAPMT window in order to illuminate one by one all the 64 pixels. At each laser positions, the charge distribution measured by the MAPMT was recorded using a CAEN V792 ADC (with a charge resolution of 1pC/channel). Typical spectra measured for two pixel of one of the MAPMTs are shown in Fig. 2. One can identify a prominent pedestal peak, followed by a broader distribution of one or more photoelectrons.

To extract the parameters of the MAPMT response, these distributions were analyzed following the method described in [2]. The ADC spectrum measured on each pixel has been fitted using the equation

$$f(q) = A \left[ e^{-\mu} P(q) + \sum_{k=1}^{N} \frac{\mu^k e^{-\mu}}{k!} G_k(q) \right] \tag{1}$$

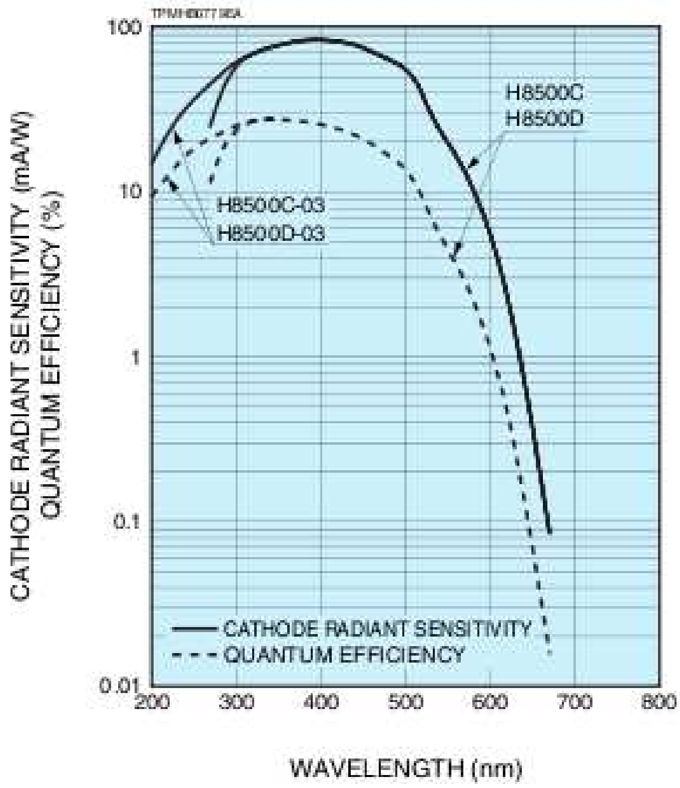


Figure 1: Quantum efficiency of the H8500C and H8500C-03 MAPMTs (dashed lines) taken from the Hamamatsu datasheets.

where $q$ is the ADC channel readout and $P(q)$ and $G_k(q)$ are functions (normalized to 1) describing the shape of the pedestal and of the $k^{th}$ photoelectron (*p.e.*) peak, respectively. Each term in the sum is weighted by the Poisson probability of having $k = 0, 1, 2, ..., N$ *p.e.* when $\mu$ is the average number of detected *p.e.*.

For the narrow measured pedestals, the gaussian shape was used, while for the *p.e.* peaks several different parametrizations have been tried. It was found that the best results (in terms of convergence of the fits and of uniformity of the function parameters) were obtained using gaussian distributions as well, even though other shapes could provide in some cases slightly better values of $\chi^2$. The free parameters of the fits are:

- the constant $A$, that, being all the factors in the sum normalized to one, gives the total number of recorded events;
- the gaussian mean ($m_0$) and width ($\sigma_0$) of the pedestal term;
- the gaussian mean ($m_1$) and width ($\sigma_1$) of the first *p.e.* peak;
- the distance ($d$) between the first and second *p.e.* peaks;
- the average number ($\mu$) of the detected *p.e.*.

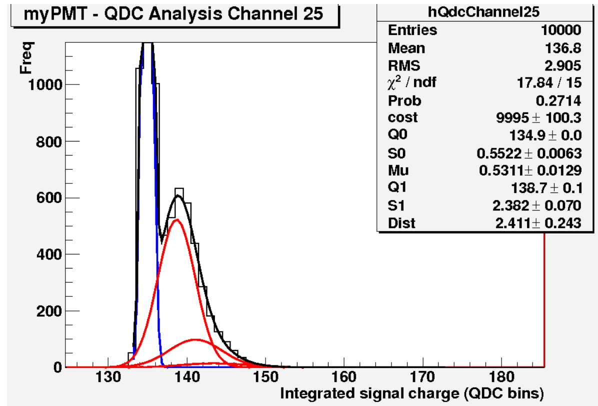


Figure 2: Two representative ADC spectra for pixel 6 (left) and 25 (right) of the CA4658 MAPMT at HV=-1000 V. The curves show the total fit (black), the pedestal (blue) and $p.e.$ (red) contributions.

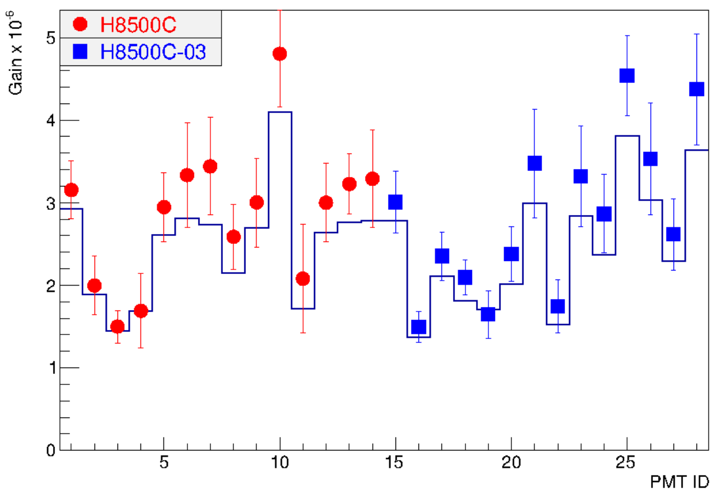


Figure 3: Average measured gain (in ADC channels) at HV = -1000 V for the 14 H8500C (red circles) and the 14 H8500C -03 (blue squares) compared with the arbitrarily normalized data sheet values from Hamamatsu (histogram). The error bars represent the RMS of the distribution on the 64 pixels.

The mean and width of the $k^{th}$ peak, for $k > 1$, are computed as $m_k = m_1 + (k-1)d$ and $\sigma_k = \sqrt{k}\sigma_1$. Tipically, the average number of $p.e.$ was less than 1, so that the total number of $p.e.$ peaks considered in the fit was chosen to be 5.

At the nominal supply voltage of -1000V, we compared our measured average MAPMT gain (in ADC channels) with the one provided by the Hamamatsu datasheets. Results are shown in Fig. 3, where red circles (blue squares) represent our data for H8500C (H8500C-03) MAPMTs and the histograms represents the Hamamatsu data (arbitrarily rescaled). Error bars on the points show the RMS of the distribution of the 64 pixels of one MAPMT. The agreement is very good, thus making us confident on our analysis technique.

Increasing the supply voltage, the separation between the signal and the pedestal im-

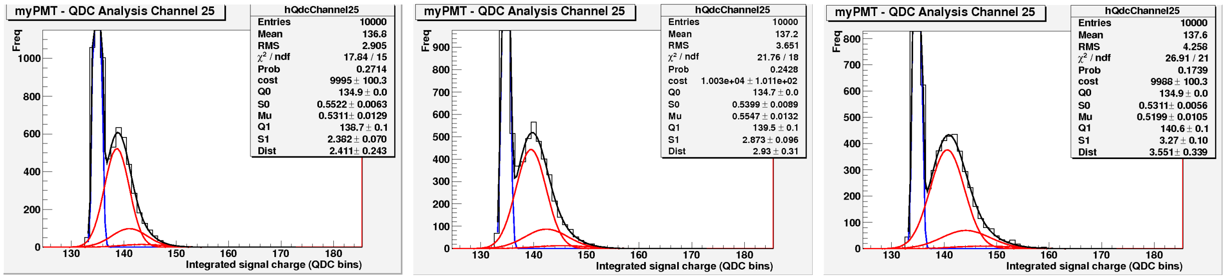


Figure 4: ADC spectra for the pixel 25 of the CA4655 MAPMT for (from left to right) HV=-1000, -1040 and -1075 V. The curves are the results of the fits, as in fig. 2

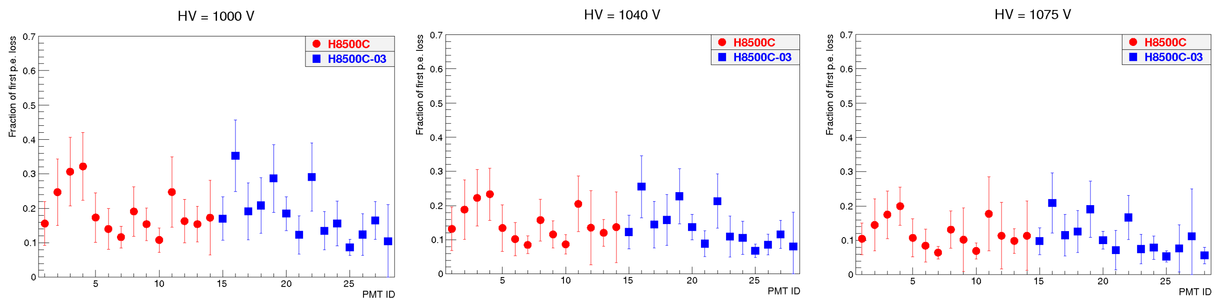


Figure 5: Fraction of the first $p.e.$ peak loss, estimated by integrating the gaussian fit above the pedestal cut, at HV=-1000 V, -1040 V and -1075V. Average values on all the 64 pixels for each of the 14 H8500C (red circles) and the 14 H8500-C03 (blue squares). The error bars represent the RMS of the distribution on all the 64 pixels of each MAPMT.

proves significantly, as shown for a pixel of one MAPMT in Fig. 4. This is a crucial point. In fact, in the CLAS12 RICH, the signal amplitude will be no more than one photon per pixel, thus it is important that the fraction of the single $p.e.$ spectrum below the pedestal peak would be as small as possible. One can estimate this loss of events by integrating the gaussian curve of the first $p.e.$ peak below a suitable cut selected to remove the ADC pedestal. Assuming a cut at $3\sigma$ above the pedestal peak, we obtained the results shown in Fig. 5 for the three supply voltages of -1000 V, -1040 V and -1075 V. We see that, at the highest voltage, except for one MAPMT, the average loss doesn't exceed 20% and that, within one RMS, all the MAPTM pixels have loss below 30%.

# 3 Cross talk

Another important parameter to be studied is the cross talk, i.e. the probability that a photon hit the MAPMT in one pixel but it is detected by one of the neighbours. To study this, we compared at the response of one pixel when it is directly illuminated by the laser beam with its response when the laser illuminates one of the four adjacent pixels. An example is shown in Fig. 6. In each histogram, the vertical red line represent the threshold to remove the pedestal ($3\sigma$ cut).

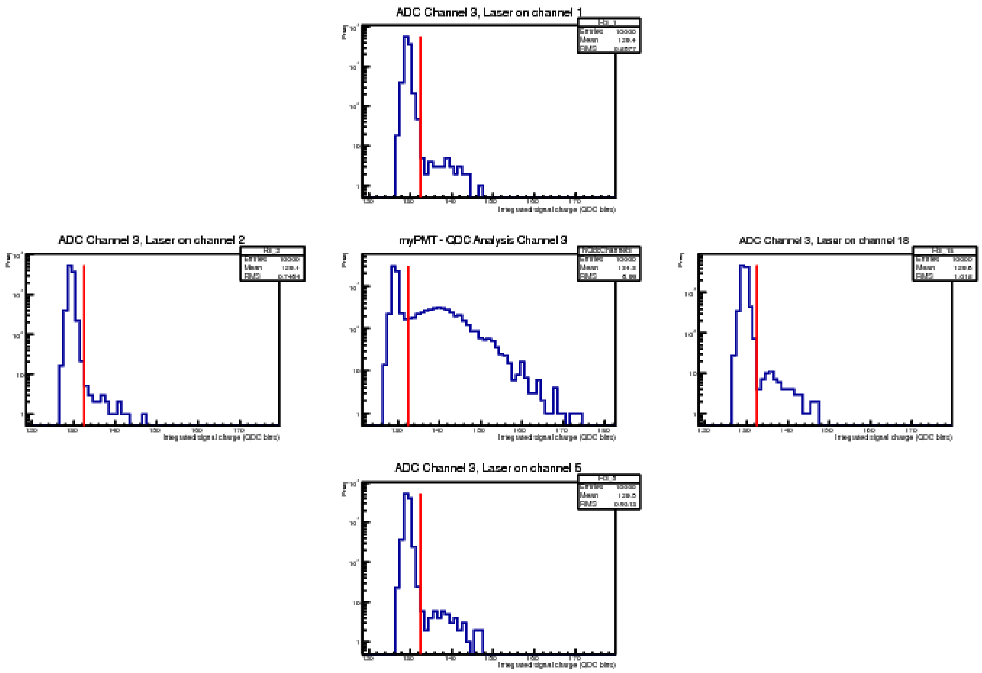


Figure 6: ADC spectrum measured by one pixel at HV=-1075V when it is directly illuminated by the laser (central histogram) and when the laser illuminates one of the four adjacent pixels (other 4 histograms). The red line indicates the threshold cut to remove the pedestal.

The cross talk is then computed as the ratio between the events above threshold when the laser illuminates the neighbour pixel with the number of events above threshold when the pixel is illuminated. In Fig. 7, we show this ratio for the 28 MAPMTs with normal (red circles) and UV enhanced (blue squares) glass window. Each point represent the average of the 64 pixels of one MAPMT and the error bar the RMS of the distribution. We found a cross talk level of few percent, in agreement with the expected performance. No strong differences have been found between the two types of H8500.

# 4 Gain analysis

In fig. 8, we show the fraction of event loss as a function of the MAPMT gain, for different threshold levels: low threshold (full squares), high threshold (empty diamonds, corresponding to a $3\sigma$ cut) and ultra-high threshold (crosses), as measured at HV=-1075V. The red full circle represent the average value of all the individual pixel gains measured in our tests. Requiring a maximum loss of $\approx 15\%$, a minimum gain of about $3 \times 10^6$ is needed, which means about $1.5 \times 10^6$ at HV=-1000V, the reference Hamamatsu high voltage. As shown in Fig. 3, only few of our MAPMT, which represent an average, random sample of the Hamamatsu production, are close to this value and none of them is clearly below.

In. Fig. 9, we show the distribution of the event loss for each of the 64 pixels of our 28 MAPMTs. A possible quality selection may be done by requiring that no more than 5% of the pixels of one MAPMTs don't exceed 30% of event loss. Only two of our MAPMTs

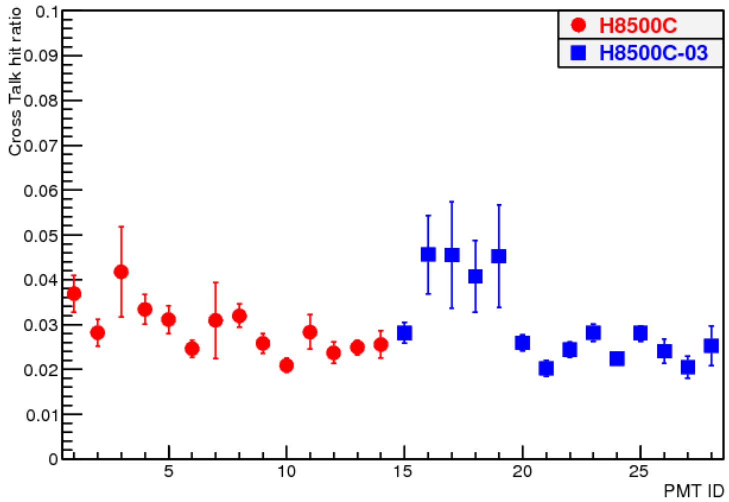


Figure 7: Cross talk fraction for the 28 MAPMTs: the points represent the average of the 64 pixels and the error bars the RMS of the distribution.

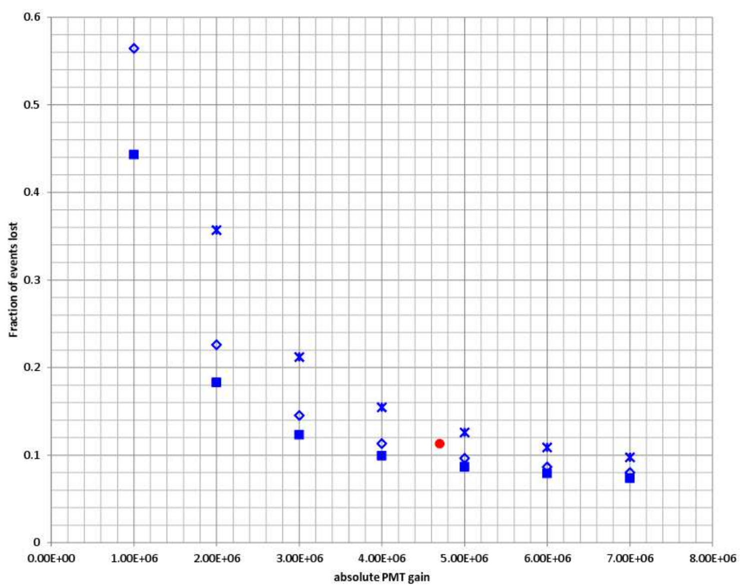


Figure 8: Fraction of event loss as a function of the MAPMT gain for three different threshold levels: low threshold (full squares), high threshold (empty diamonds, corresponding to a $3\sigma$ cut) and ultra-high threshold (crosses), as measured at HV=-1075V.

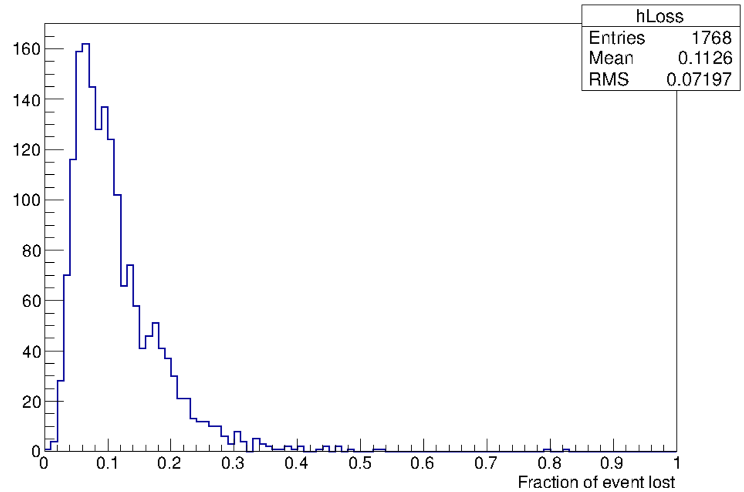


Figure 9: Distribution of the pixel gains measured at HV=-1075V for all the 28 MAPMTs tested.

would be discarded according to this criterium, corresponding to less than 10% of the tubes tested.

# 5 Dark current analysis

The MAPMT dark current is a source of uncorrelated background and can impact on the detector performance. A dark current measurement is provided by Hamamatsu for each H8500C. The dark current measured by Hamamatsu is for the entire MAPMT, i.e. for a single channel this number needs to be divided by 64. First of all, a correlation of dark current and PMT gain is investigated. However, no clear correlation could be established (see Fig. 10). Nevertheless, it is obvious that a few MAPMTs exhibit excessive dark current values which need to be rejected in a RICH application.

The average gain and dark current values of the 28 MAPMTs, see Fig. 11, show no significant difference between standard and UV entrance window types. The average dark count rate $R_{dc}$ can be computed from the dark current, assuming that essentially all dark counts are single photoelectron signals, by

$$R_{dc} = \frac{I_{dc}dt}{G \times e}, \tag{2}$$

with $I_{dc}$ being the dark current, the time interval $dt$ which is set to 1 s to get $R_{dc}$ in counts per second, $G$ is the MAPMT gain, and $e$ is the elementary charge. In this case the average dark count rate is between 500–1000 cps except for MAPMTs with excessive dark current.

The cross talk measurements (see Sect. 3) have been also analysed with respect to the dark current. In Fig. 12, we show the cross talk level of the 28 MAPMTs measured with HV=-1075V as a function of the dark current quoted by Hamamatsu. No strong dependences have been found.

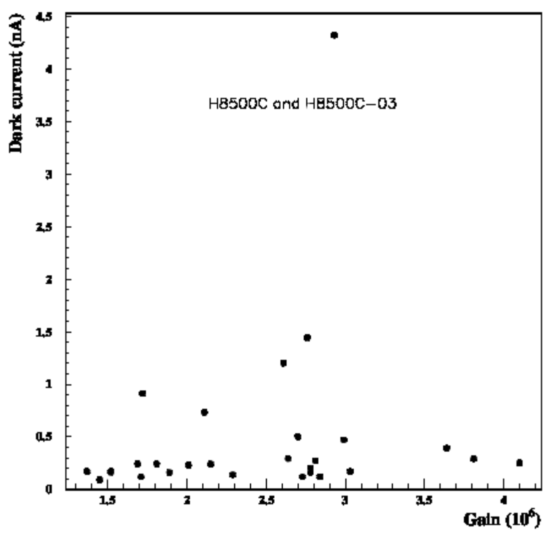


Figure 10: Dark current provided by Hamamatsu as a function of MAPMT gain.

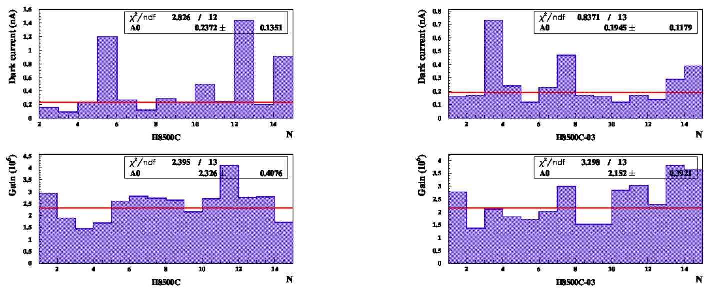

Figure 11: Average gain and dark current for 14 H8500C (left) and 14 H8500C-03 with UV window (right). The average dark current and gain values are indicated by the red line.

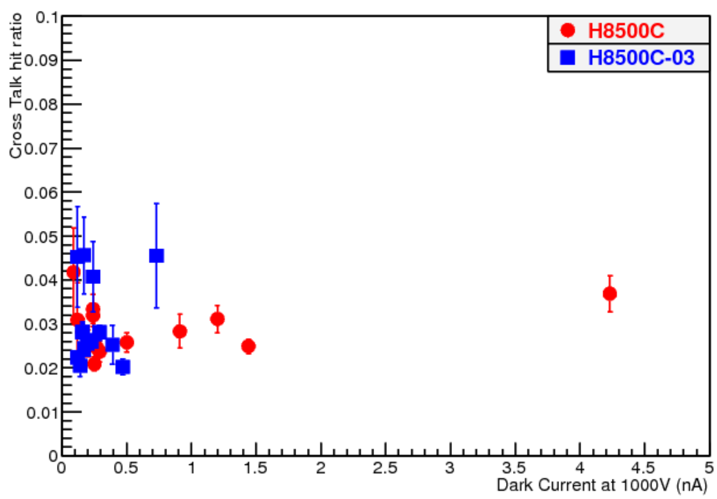


Figure 12: Cross talk fraction for the 28 MAPMTs as a function of the dark current quoted by Hamamatsu: the points represent the average of the 64 pixels and the error bars the RMS of the distribution.

# References

[1] NIM, in preparation

[2] R. Perrino *et al.*, Nucl. I. and Meth. **A457** (2001) 571.